

# Spectroscopic Characterisation of $250\mu\text{m}$ -Selected Hyper-Luminous Star Forming Galaxies

C. M. Casey<sup>1,2\*</sup>, S. C. Chapman<sup>1</sup>, Ian Smail<sup>3</sup>, S. Alaghband-Zadeh<sup>1</sup>,  
M. S. Bothwell<sup>1</sup>, A. M. Swinbank<sup>3</sup>

<sup>1</sup> *Institute of Astronomy, Madingley Road, Cambridge, CB3 0HA*

<sup>2</sup> *Institute for Astronomy, University of Hawai'i, 2680 Woodlawn Dr, Honolulu, HI 96822, USA*

<sup>3</sup> *Institute for Computational Cosmology, Durham University, South Road, Durham DH1 3LE*

Submitted 12 July 2010, Revised with minor corrections from referee, 10 September 2010. Version date 21 November 2018

## ABSTRACT

We present near-infrared spectroscopic observations from VLT ISAAC of thirteen  $250\mu\text{m}$ -luminous galaxies in the CDF-S, seven of which have confirmed redshifts which average to  $\langle z \rangle = 2.0 \pm 0.4$ . Another two sources of the 13 have tentative  $z > 1$  identifications. Eight of the nine redshifts were identified with  $\text{H}\alpha$  detection in H- and K-bands, three of which are confirmed redshifts from previous spectroscopic surveys. We use their near-IR spectra to measure  $\text{H}\alpha$  line widths and luminosities, which average to  $415 \pm 20 \text{ km s}^{-1}$  and  $3 \times 10^{35} \text{ W}$  (implying  $\text{SFR}_{\text{H}\alpha} \sim 200 \text{ M}_{\odot} \text{ yr}^{-1}$ ), both similar to the  $\text{H}\alpha$  properties of SMGs. Just like SMGs,  $250\mu\text{m}$ -luminous galaxies have large  $\text{H}\alpha$  to far-infrared (FIR) extinction factors such that the  $\text{H}\alpha$  SFRs underestimate the FIR SFRs by  $\sim 8$ -80 times. Far-infrared photometric points from observed  $24\mu\text{m}$  through  $870\mu\text{m}$  are used to constrain the spectral energy distributions (SEDs) even though uncertainty caused by FIR confusion in the BLAST bands is significant. The population has a mean dust temperature of  $T_d = 52 \pm 6 \text{ K}$ , emissivity  $\beta = 1.73 \pm 0.13$ , and FIR luminosity  $L_{\text{FIR}} = 3 \times 10^{13} L_{\odot}$ . Although selection at  $250\mu\text{m}$  allows for the detection of much hotter dust dominated HyLIRGs than SMG selection (at  $850\mu\text{m}$ ), we do not find any  $\gtrsim 60 \text{ K}$  ‘hot-dust’ HyLIRGs. We have shown that near-infrared spectroscopy combined with good photometric redshifts is an efficient way to spectroscopically identify and characterise these rare, extreme systems, hundreds of which are being discovered by the newest generation of IR observatories including the *Herschel Space Observatory*.

**Key words:** galaxies: evolution – galaxies: high-redshift – galaxies: infrared – galaxies: starbursts

## 1 INTRODUCTION

Submillimetre Galaxies (SMGs) contribute significantly to the rapid buildup of stellar mass in the Universe at  $z \sim 2$ . However, their selection at  $850\mu\text{m}$  is inherently biased towards colder-dust sources (Eales et al. 2000; Blain et al. 2004). Recent work (e.g. Chapman et al. 2004; Casey et al. 2009c) has demonstrated that  $850\mu\text{m}$ -faint, high-redshift Ultraluminous Infrared Galaxies (ULIRGs) exist and may contribute significantly to the cosmic star formation rate density at its peak. Casey et al. (2009c) describe a population of  $70\mu\text{m}$  luminous galaxies at  $z \sim 1.5$  whose infrared luminosities exceed  $\sim 10^{12} L_{\odot}$  but are  $850\mu\text{m}$ -faint

due to hotter characteristic dust temperatures. Sparse infrared data, particularly in the  $50$ - $500\mu\text{m}$  wavelength range, along with poor volume density constraints have limited the interpretation of these submm-faint ULIRGs. Similar studies of other infrared-luminous galaxy populations, selected at  $24\mu\text{m}$ ,  $350\mu\text{m}$  or  $1.2\text{mm}$  for example, present even more evidence for diverse populations of luminous, dusty starbursts at  $z \gtrsim 1$  which do not necessarily intersect (see Dey et al. 2008; Bussmann et al. 2009; Younger et al. 2009).

The arrival of new infrared (IR) instruments—including BLAST (the Balloon-borne Large-Aperture Submillimeter Telescope Pascale et al. 2008), SCUBA2, LABOCA, and the *Herschel Space Observatory*—has opened up more extensive studies of these distant starbursts. BLAST’s deep mapping of the Extended *Chandra* Deep Field South (ECDF-

\* Hubble Fellow; cmcasey@ifa.hawaii.edu

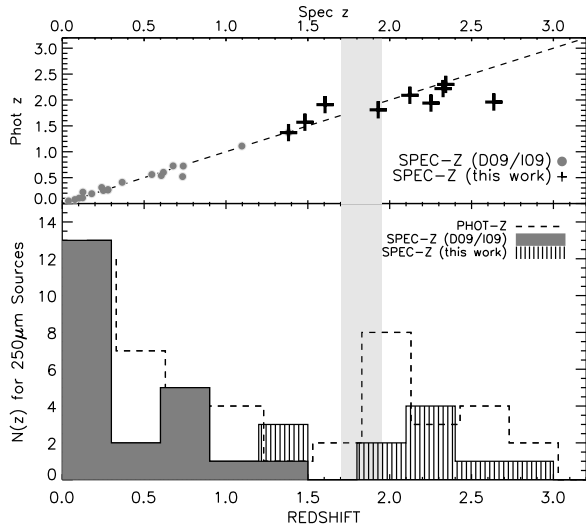


**Figure 1.** The redshift distribution of BLAST  $250\mu\text{m}$  sources, including the low-redshift spectroscopically identified sources in D10 and I10 (*gray points/histogram*). Our spectroscopic sample has a mean redshift  $2.0 \pm 0.4$  (*black crosses, lined histogram*), which fills in much of the high-redshift subsample of  $250\mu\text{m}$ -bright objects. The distribution in photometric redshifts is illustrated as the dashed line histogram and are good to  $\sim 12\%$ . The light gray vertical stripe blocks out the redshift regime where near-IR spectroscopy cannot confirm redshifts since  $\text{H}\alpha$  falls between H and K bands.

S) at  $250\mu\text{m}$ ,  $350\mu\text{m}$ , and  $500\mu\text{m}$  has, for the first time, led to  $z \sim 2$  ULIRG selection near the peak of their SED. Ivison et al. (2010) and Dunlop et al. (2009) describe the selection of these  $250\mu\text{m}$  sources, along with their radio and  $24\mu\text{m}$  counterparts, in detail and match sources to photometric redshifts derived from the extensive ECDF-S multi-wavelength data. We also make use of longer wavelength constraints from the LABOCA  $870\mu\text{m}$  survey of the ECDF-S (Weiß et al. 2009). While most low redshift ( $z \lesssim 0.8$ )  $250\mu\text{m}$  sources have spectroscopic identifications, none of the suspected high-redshift sources had spectroscopic redshifts.

This paper presents new VLT ISAAC spectroscopic observations of thirteen BLAST  $250\mu\text{m}$  sources with  $z_{\text{phot}} > 1$ . With spectroscopic redshifts, we constrain the FIR dust SED (implying that they are HyLIRGs with  $L_{\text{FIR}} \gtrsim 10^{13} L_{\odot}$ ), measure dust temperatures, blackbody emissivity, FIR luminosities,  $\text{H}\alpha$  luminosities and AGN/metal lines, and constrain the FIR/radio correlation for these high- $z$  galaxies. Throughout we use a  $\Lambda_{\text{CDM}}$  cosmology (Hinshaw et al. 2009) with  $H_0 = 71 \text{ km s}^{-1} \text{ Mpc}^{-1}$  and  $\Omega_0 = 0.27$ .

## 2 OBSERVATIONS & RESULTS

Longslit spectroscopic observations of  $250\mu\text{m}$  sources were obtained in November 2009 on the Very Large Telescope (VLT) Infrared Spectrometer And Array Camera (ISAAC) under excellent seeing conditions ( $0.3\text{--}0.7''$  in K-band). Spectroscopic candidates were chosen from the Ivison et al. (2010) and Dunlop et al. (2009) (hereafter I10 and D10) ECDF-S BLAST Deep map samples (RMS sensitivity

$\sigma_{250} = 11 \text{ mJy}$ ) with photometric redshifts above  $z = 1$  or undefined photometric redshifts (the latter caused by a lack of high quality photometry). I10 selected sources at  $> 5\sigma$ , having folded in the confusion noise ( $\sim 21 \text{ mJy}$ ), resulting in flux densities  $S_{250} > 59 \text{ mJy}$ . D10 selected sources at  $> 3\sigma$  without accounting for the confusion noise, so their source list has  $S_{250} > 33 \text{ mJy}$ . All had reliable  $24\mu\text{m}$  and/or radio counterparts, which were then matched to K-band sources (with offsets  $< 1''$  to the radio/ $24\mu\text{m}$  centroid) in archival MUSYC data (Gawiser et al. 2006) for VLT spectroscopic targeting. The resulting candidate object list contained 20 sources.

We refer the reader to D10 and I10 for the analysis of the BLAST  $250\mu\text{m}$  CDF-S map and source selection, as well as some source properties derived from ancillary data. The two papers present different detection thresholds (which are discussed in more detail as they relate to source density estimations in section 3.1) and also use different counterpart identification methods to identify sources for photometric redshift fitting. D10 uses  $24\mu\text{m}$  counterpart matching, while I10 uses 1.4 GHz radio matching. In general radio matching is much more reliable assuming the FIR/radio correlation holds (Helou et al. 1985) as there are far fewer potential counterparts and good reason to suspect a FIR-bright source is also radio-bright. Identification at  $24\mu\text{m}$  is a less reliable alternative due to the large IR beamsize and density of sources. We caution the reader that our K-band identifications are nearest neighbours to the radio and  $24\mu\text{m}$  counterpart astrometry of D10 and I10 and that there is minor potential for misidentified counterparts. The offsets between  $250\mu\text{m}$  peaks and K-band sources (which are effectively equivalent to the radio/ $24\mu\text{m}$  positions) range from  $1\text{--}16''$ , averaging to about  $7''$ , which is well within the beamsize of  $250\mu\text{m}$  observations, however it is not possible to know if the counterparts have been identified correctly without high-resolution FIR observations (e.g. Younger et al. 2010).

We observed 13 of the 20  $z_{\text{phot}} > 1$   $250\mu\text{m}$  sources searching for  $\text{H}\alpha$  or  $[\text{OIII}]$  in J, H, and K bands. The band of observations was primarily chosen based on the galaxies' photometric redshifts (where galaxies with  $z_{\text{phot}} > 2$  were observed in K-band and at  $z_{\text{phot}} < 1.8$  in H-band, and in J-band for the intermediate region). Galaxies were observed individually under varying seeing conditions which ranged from  $0.3\text{--}0.7''$  seeing in K-band. Since all galaxies here are assumed to be unresolved, we varied the slit width according to seeing conditions, minimising it when possible to reduce sky line contamination. Galaxies were centred on the  $2'$  long slit and observed in ABBA nodding mode with a  $15''$  nod. On occasion, two candidates were within a  $2'$  separation and placed on the same slit, with the maximum possible nod distance, which was sometimes  $5\text{--}10''$ . Data reduction was completed with ESO software combined with IRAF and our own IDL-based routines to obtain 1D and 2D wavelength calibrated spectra.

Only 13 of the sources were observed due to telescope time constraints. Nine of the 13 have spectroscopic redshifts, seven of which are secure. Three of these seven sources (J033246, J033152, and J033243) were already identified in previous spectroscopic surveys using the Very Large Telescope/Focal Reducer and low dispersion Spectrograph 2 and the Gemini Near-Infrared Spectrograph (Vanzella et al. 2008; Kriek et al. 2008) at  $z = 1.382$ ,  $2.336$  and  $2.122$  re-

spectively. Our measured redshifts confirm these observations. Six of the seven secure redshifts and the two tentative redshifts were measured from H $\alpha$  detection (at  $>4\sigma$  H $\alpha$  signal-to-noise). One of the eight H $\alpha$  redshifts (J033129) would nominally be tentative, but it was spectroscopically identified in the rest-UV independently; the ninth secure redshift which is not based on H $\alpha$  (J033151) has absorption features in the K-band at  $\sim 1.599$  which agree with a rest-UV redshift of 1.605 obtained independently (Swinbank, private communication). The lines were identified as H $\alpha$  using a combination of photometric redshift consistency and a lack of other line features (which would instead identify the line as [OII] or [OIII], in the case of [NII] or SII detection). The four sources which were not identifiable in emission either have very weak emission features or lie at redshifts in the range  $1.7 < z < 2.0$ ; H $\alpha$  at these redshifts falls between H- and K- bands and is thus not detectable with near-IR spectroscopy.

The nine galaxies have a mean redshift  $z = 2.0 \pm 0.4$ , and their redshift distribution, with respect to other 250 $\mu\text{m}$  sources, is shown in Figure 1. We determine that their photometric redshifts (derived in D10 and in Rafferty et al., in prep, for I10 sources) are good to  $dz/(1+z) \lesssim 12\%$ , and we emphasise that this relatively small error implies that near-IR spectroscopic followup for ULIRGs with good photometric redshifts is efficient. Table 1 summarises the galaxies properties and Figure 2 shows their ISAAC spectra for those which were spectroscopically identified. The galaxies' names are derived from their positions in the K band.

The spectra in Figure 2 are framed around the H $\alpha$  emission for every source except J033151. Regions where emission lines in the sky's infrared spectrum<sup>1</sup> are significant (with flux densities in excess of  $\sim 5\gamma \text{ s}^{-1} \text{ nm}^{-1} \text{ arcsec}^{-2} \text{ m}^{-2}$  where  $\gamma$  represents photons) are masked out in both 1D and 2D spectral renditions. The width of these sky lines varied according to the slit width of each observation, which varied from 0.3-0.8''.

We use the publicly released smoothed maps of the BLAST ECDF-S (Devlin et al. 2009) to derive 350 $\mu\text{m}$  and 500 $\mu\text{m}$  flux densities for the D10 sample (both 350 $\mu\text{m}$  and 500 $\mu\text{m}$  flux densities are published for the I10 sample). We use the K-band astrometry (where the VLT slit was placed) as position priors to extract BLAST flux densities since the maps are dominated by confusion noise. We note however, that because the maps are highly confused, they are likely to suffer from flux boosting on individual sources, especially for the fainter 250 $\mu\text{m}$  sources; see Chapin et al. (2010) for a detailed analysis of source extraction, confusion limitations with BLAST data, and SED fitting.

The fluxes in Table 1 are not corrected for deboosting, but we do apply corrections when fitting FIR SEDs and deriving  $L_{\text{FIR}}$ ,  $T_{\text{dust}}$  and  $\beta$ . We use the signal-to-noise ratio of the 250 $\mu\text{m}$  detections to determine the deboosting factor which corrects for the Eddington bias and boosting by confusion noise, as in Eales et al. (2009), figure A2. This results in flux densities which are  $\sim 55$ -75% of the original measured values for the BLAST bands given in Table 1.

We do not correct 870 $\mu\text{m}$  LABOCA points for deboosting since the 870 $\mu\text{m}$  flux densities are less likely to be boosted by flux from adjacent sources. This is because the sources which boost a high-redshift galaxy's 250-500 $\mu\text{m}$  flux density are far more likely to sit at lower redshifts than at higher redshifts (where the surface density of sources is more rare). These low redshift sources are also unlikely to be bright at 870 $\mu\text{m}$  given typical blackbody SED shapes at low- $z$ . We recognise that our application of a deboosting factor to the BLAST bands and not the LABOCA data is a simplification of a complex issue, but we consider it the most realistic constraint on the FIR flux densities given the data which are available. We do not deboost the *Spitzer* MIPS photometry at shorter wavelengths since the source surface density at  $\sim 70\mu\text{m}$  is similar to the source density at  $\gtrsim 200\mu\text{m}$ , yet the relative beam size is much smaller at shorter wavelengths.

We choose not to propagate the uncertainty in the FIR deboosting factor (which is estimated to be as large as 50% at low 250 $\mu\text{m}$  S/N) into the SED uncertainty because the deboosting factor is not independent between bands. Despite the large uncertainty, the FIR flux densities for individual sources would be deboosted by similar factors. A correlated deboosting factor between bands would imply less uncertainty in derived  $T_{\text{dust}}$  or  $\beta$  than blindly adopting the deboost uncertainties. We test the correlation of the deboosting factor by using the FIR colours ( $S_{250}/S_{350}$  and  $S_{250}/S_{500}$ ) of *Herschel* SPIRE and PACS sources (Amblard et al. 2010). Using Monte Carlo tests, we remove the contribution of a single potential boosting source by subtraction of an arbitrary 250 $\mu\text{m}$  flux and the associated 350 $\mu\text{m}$  and 500 $\mu\text{m}$  fluxes associated with the colours of a randomly selected galaxy from the Amblard et al. (2010) sample. We find that the FIR luminosity does not vary by more than  $\pm 0.1$  dex and that dust temperature varies by about  $\pm 9$  K. If two contaminating boosting sources are incorporated with different FIR colour properties, the variance on the fitted  $L_{\text{FIR}}$  and  $T_{\text{dust}}$  decreases further. We discuss the impact that the deboosting factor uncertainty has on our final conclusions more in § 3.5.

We measure 870 $\mu\text{m}$  flux densities (at the K-band positions) from the LABOCA map of ECDF-S (Weiß et al. 2009). Six sources have  $S_{870} \gtrsim 4$  mJy and are listed in Weiß et al. (2009). J033246 is claimed as an SMG in D10, but its 870 $\mu\text{m}$ -peak is  $>30''$  away from its K-band position. This implies that 7/13 ( $\sim 53\%$ ) of our sample are submm-faint and would be excluded from traditional SMG surveys. All galaxies except J033212 are also radio detected in VLA data at  $>30 \mu\text{Jy}$ .

The galaxies' rest-frame near-IR photometry is consistent with stellar emission, from which we derive stellar masses from rest-frame *H*-band (Table 2), using the methods described by Hainline et al. (2009). Measuring the absolute magnitude of a galaxy near its 1.6 $\mu\text{m}$  "stellar bump" provides the most accurate measure of its stellar mass, however it is reliant on the assumption of a constant mass to light ratio (here we assume  $M/L = 3.2$ ), reddening properties, and minimal AGN contribution to near-IR flux. The stellar mass estimates are uncertain by  $\sim 0.3$  dex. The near-IR photometry is also be used to infer AGN content, since a flux excess at 8 $\mu\text{m}$  (significantly above stellar population model fits) is indicative of power law emission from an AGN. None of our sources have  $>2\sigma$  8 $\mu\text{m}$  flux excesses.

<sup>1</sup> See the Gemini Observatories IR Background Spectra page (<http://www.gemini.edu/?q=node/10787>) for example sky spectra.

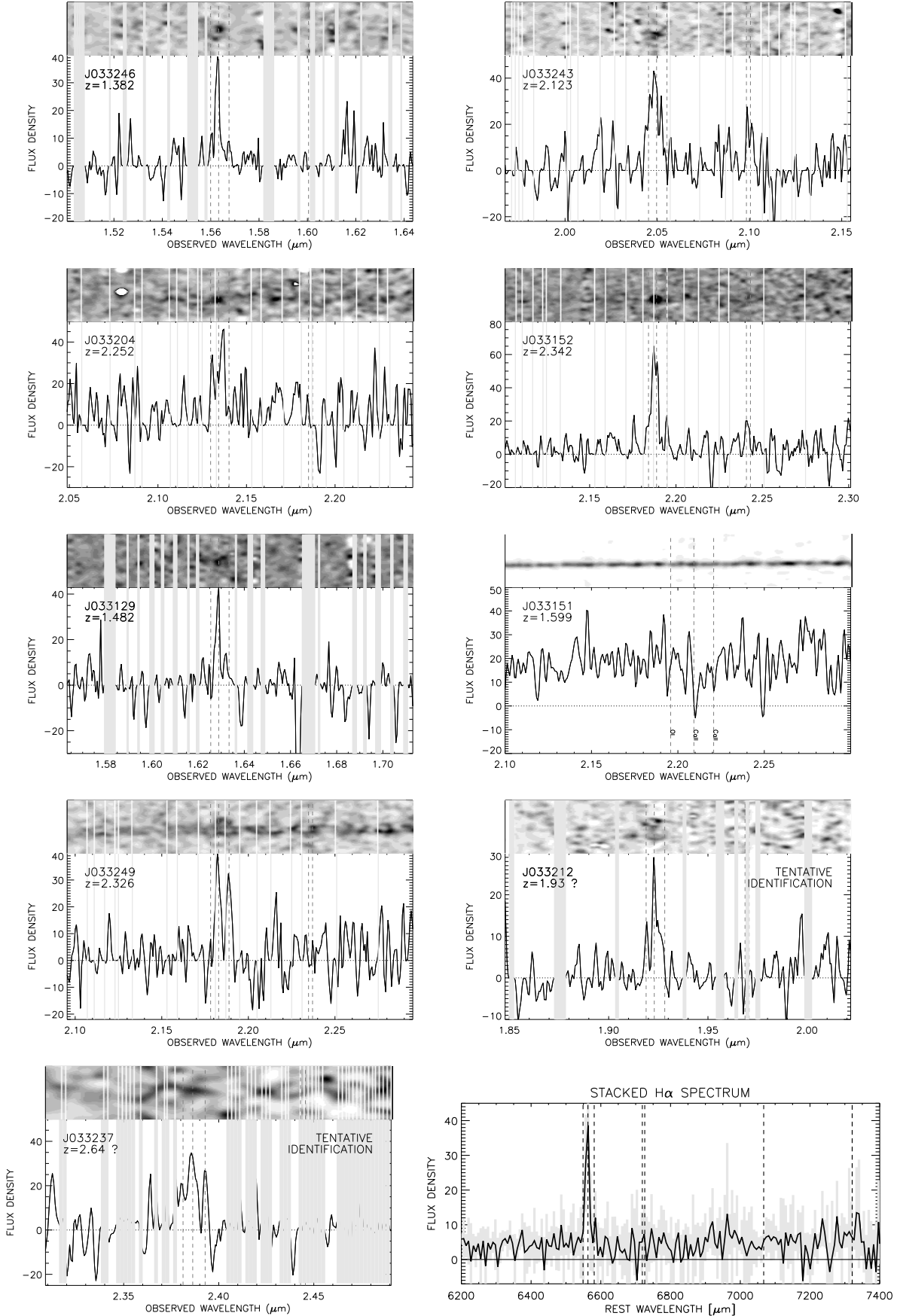


**Figure 2.** The VLT ISAAC spectroscopy of nine  $250\mu\text{m}$  BLAST sources around their  $\text{H}\alpha$  emission ( $0.63\text{-}0.69\mu\text{m}$  rest wavelength), except in the case of J033151 when no  $\text{H}\alpha$  observations were obtained. The first seven sources have secure redshifts, the next two are tentative, and the last is a stacked  $\text{H}\alpha$  spectrum for the six secure  $\text{H}\alpha$  sources. Observations were taken in H or K band, and both 2d and 1d projections are shown for clarity; scaling is optimised for viewing spectral features which are marked by vertical dashed lines (e.g.  $\text{H}\alpha$ , NII). The 2d spectra show an angular scale of  $12''$  top to bottom and the 1d spectra are extracted within  $0.6''$ . Sky line emission

**Table 1.** Multi-wavelength properties of BLAST 250  $\mu$ m Galaxies

NAME <sup>a</sup>	ID <sup>b</sup>	$z_{\text{spec}}$	$z_{\text{phot}}$	$S_{24}$ ( $\mu$ Jy)	$S_{250}$ (mJy)	$S_{350}^d$ (mJy)	$S_{500}^d$ (mJy)	$S_{1.4}$ ( $\mu$ Jy)	$S_{870}^d$ (mJy)	CLASS <sup>e</sup>	$L_{\text{FIR}}$ ( $10^{13} L_{\odot}$ )	$T_{\text{dust}}$ (K)	$\beta$	$q_{\text{IR}}^f$
<b>DETECTIONS</b>														
J033129.874-275722.40	J033129	1.482	1.57	270	91.6 $\pm$ 11.0	54.4 $\pm$ 8.7	46.3 $\pm$ 6.2	144 $\pm$ 16	5.0 $\pm$ 1.5	SMG	(1.2 $^{+0.7}_{-0.4}$ )	45.9 $\pm$ 3.9	1.2 $\pm$ 0.3	2.7 $\pm$ 0.5
J033151.088-274436.91	J033151	1.599	1.91	520	74.0 $\pm$ 10.8	63.8 $\pm$ 8.5	37.4 $\pm$ 5.9	96 $\pm$ 13	4.6 $\pm$ 1.4	SMG	(2.2 $^{+1.4}_{-0.9}$ )	47.1 $\pm$ 3.0	1.6 $\pm$ 0.3	3.0 $\pm$ 0.8
J033152.090-273926.32	J033152	2.342 <sup>c</sup>	2.30	200	78.3 $\pm$ 11.0	64.3 $\pm$ 8.6	53.1 $\pm$ 6.0	965 $\pm$ 16	2.4 $\pm$ 1.4	SFRG	(8.1 $^{+6.0}_{-3.4}$ )	44.5 $\pm$ 3.0	2.6 $\pm$ 0.3	2.2 $\pm$ 0.5
J033204.849-274647.27	66	2.252	1.94	540	64.3 $\pm$ 10.9	62.0 $\pm$ 8.4	22.4 $\pm$ 6.0	126 $\pm$ 12	7.9 $\pm$ 1.4	SMG	(4.0 $^{+1.0}_{-0.8}$ )	56.7 $\pm$ 5.2	1.3 $\pm$ 0.4	2.8 $\pm$ 0.6
J033243.209-275514.38	318	2.123 <sup>c</sup>	2.09	510	30.1 $\pm$ 10.9	32.4 $\pm$ 8.5	17.8 $\pm$ 6.0	92 $\pm$ 10	5.7 $\pm$ 1.4	SMG	(1.4 $^{+2.5}_{-0.9}$ )	56.9 $\pm$ 8.6	0.8 $\pm$ 0.7	1.6 $\pm$ 0.4
J033246.329-275327.01	1293	1.382 <sup>c</sup>	1.37	200	28.1 $\pm$ 10.9	25.3 $\pm$ 8.6	14.7 $\pm$ 5.9	91 $\pm$ 7	-1.3 $\pm$ 1.4	SFRG	(0.4 $^{+0.1}_{-0.1}$ )	53.0 $\pm$ 12.9	0.8 $\pm$ 0.7	2.5 $\pm$ 0.7
J033249.352-275845.07	J033249	2.326	2.22	320	101.2 $\pm$ 10.9	66.4 $\pm$ 8.6	22.6 $\pm$ 6.0	216 $\pm$ 16	2.5 $\pm$ 1.3	SFRG	(8.1 $^{+3.9}_{-2.6}$ )	56.7 $\pm$ 4.5	2.1 $\pm$ 0.3	2.8 $\pm$ 0.3
<b>TENTATIVE</b>														
J033212.866-274640.89	193	1.93	1.81	40	46.0 $\pm$ 10.9	33.2 $\pm$ 8.5	8.6 $\pm$ 6.0	<40	-0.5 $\pm$ 1.4	SFRG	(2.2 $^{+4.3}_{-1.4}$ )	42.7 $\pm$ 9.4	=2.0	<3.20
J033237.731-275000.41	503	2.64	1.96	210	38.0 $\pm$ 10.9	20.0 $\pm$ 8.6	16.3 $\pm$ 6.0	170 $\pm$ 8	2.6 $\pm$ 1.4	SFRG	(3.5 $^{+1.4}_{-2.4}$ )	46.0 $\pm$ 8.4	=2.0	2.4 $\pm$ 0.4
<b>NON-DETECTIONS</b>														
J033221.624-275623.49	158	...	1.85	510	54.9 $\pm$ 10.9	28.5 $\pm$ 8.4	31.2 $\pm$ 6.0	38 $\pm$ 8	4.8 $\pm$ 1.4	SMG	...	...	...	...
J033317.754-274605.96	J033318	...	2.06	430	79.9 $\pm$ 10.8	72.5 $\pm$ 8.6	51.4 $\pm$ 5.9	100 $\pm$ 14	4.3 $\pm$ 1.4	SFRG	...	...	...	...
J033128.792-273916.85	J033128	...	...	460	105.3 $\pm$ 11.1	69.6 $\pm$ 8.7	39.8 $\pm$ 6.3	35 $\pm$ 8	4.5 $\pm$ 1.5	SFRG	...	...	...	...
J033248.011-275416.42	593	...	>2.80	<30	18.8 $\pm$ 11.0	33.5 $\pm$ 8.6	12.2 $\pm$ 6.0	44 $\pm$ 8	9.3 $\pm$ 1.4	SMG	...	...	...	...

**Table Notes.** <sup>a</sup> Galaxies are split into three categories: ‘detections’ (sources which have reliable redshift identifications), ‘tentative’ (poor quality redshift identifications), or ‘non-detections’ (no visible emission features). All redshift identifications are based on H $\alpha$  detection except J033151. The galaxies with ‘tentative’ identifications are included in all figures and tables of this paper but are excluded from the primary analysis points in section 3 so as not to affect the interpretation of this paper.

<sup>b</sup> ID is the identification of the 250 $\mu$ m source taken from D10 or I10. Those from I10 are of the form J033XXX and correspond to the first half of the BLAST name given in table 1 of I10. Those from D10 appear as two to four digit numbers and can be found as the BLAST IDs in table 1 of D10.

<sup>c</sup> Three sources have confirmed redshifts from previous spectroscopic surveys (Vanzella et al. 2008; Kriek et al. 2008).

<sup>d</sup>  $S_{350}$ ,  $S_{500}$ , and  $S_{870}$  are measured directly from BLAST/LABOCA ECDF-S maps at their respective wavelengths, using the K-band astrometry for sources in the D10 sample, and 24 $\mu$ m and 1.4 GHz flux densities are based on nearest neighbour matching (described in I10). The flux densities at 250 $\mu$ m, 350 $\mu$ m and 500 $\mu$ m have not been corrected for flux boosting, and their uncertainties here only represent instrumental uncertainty; they should be combined in quadrature with the confusion noise ( $\sim$ 21 mJy) for an accurate representation of flux uncertainty.

<sup>e</sup> A galaxy’s class is either SMG (submm galaxy) or SFRG (submm-faint radio galaxy) based on its inclusion as a significant detection in the Weiß et al. (2009) sample, i.e. if its 870 $\mu$ m flux density is  $\gtrsim$  4 mJy.

<sup>f</sup> The ratio of IR luminosity to radio luminosity (as calculated in I10 using  $\alpha = 0.75$ , see their section 2.2),  $q_{\text{IR}}$ , is given in the last column.

Two of the 13 observed sources, J033151 and J033152, are X-ray detected above the luminosities which would correspond with their star formation rates ( $L_X \gtrsim 10^{44}$  erg s $^{-1}$ ). Only one individual source shows obvious signs of containing a luminous AGN, from its radio flux excess and detection in the X-rays: J033152. From this AGN estimator (and the analysis in the ensuing section about H $\alpha$  properties), we infer roughly that 20 $\pm$ 15% of 250 $\mu$ m-bright sources have signs of dominant AGN.

## 2.1 H $\alpha$ Properties

We measure H $\alpha$  line widths and [NII]/H $\alpha$  ratios in order to infer AGN content from the six BLAST sources for which we have secure H $\alpha$  observations (i.e. not including J033151). After deconvolving the measured full width half maxima (FWHM) with the instrumental resolution measured from skylines in the vicinity of H $\alpha$  ( $\sim$ 6.5 $\text{\AA}$  in K-band and  $\sim$ 4.4 $\text{\AA}$  in H-band) we find that our H $\alpha$  lines have an average rest-frame FWHM of 415 $\pm$ 20 km s $^{-1}$  and span the range 150-800 km s $^{-1}$  (for the six galaxies with secure H $\alpha$  detections). The individual H $\alpha$  properties of each galaxy are given in Table 2. We plot the H $\alpha$  FWHM against H $\alpha$  luminosity

in Figure 3. The H $\alpha$ -inferred star formation rates average to 210 $\pm$ 160 M $_{\odot}$  yr $^{-1}$ , which requires a substantial extinction factor to account for the star formation observed in the FIR (on the order of 2000 M $_{\odot}$  yr $^{-1}$ ). The mean SFR $_{\text{FIR}}$ /SFR $_{\text{H}\alpha}$  ratio for the sample is 36 $\pm$ 22, which is comparable to the ratio for the SMG population of Swinbank et al. (2004) of 31 $\pm$ 15. The subset of our sample which is submm-faint (SFRGs) also have similar SFR ratios, averaging 37 $\pm$ 24.

For the six galaxies which have secure H $\alpha$  observations, a stacked spectrum is shown in Figure 2 which we use to measure the aggregate line emission properties of the sample. The H $\alpha$  line width of the stacked spectrum is 530 $\pm$ 280 km s $^{-1}$  (statistically indistinguishable from the individual H $\alpha$  measurements or the mean SMG line width, 390 km s $^{-1}$ ), and a line luminosity corresponding to a star formation rate of 190 M $_{\odot}$  yr $^{-1}$ . The line width is slightly larger than the mean line width for the sample likely due to signal-to-noise limitations of the original data. Both line width measurements, 415 km s $^{-1}$  and 530 km s $^{-1}$ , are consistent with the dynamics of active star forming HII regions, except the high FWHM outlier: J033243 at  $z = 2.123$  with FWHM = 800 km s $^{-1}$ . J033243 is also the second brightest H $\alpha$  emitter with a high H $\alpha$  implied SFR, 335 M $_{\odot}$  yr $^{-1}$ ; its

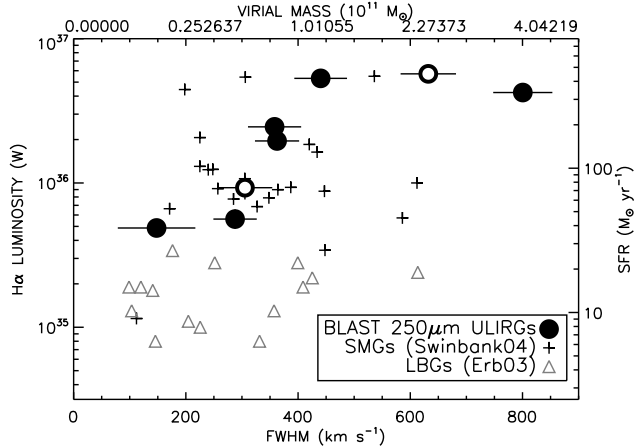


**Figure 3.** The relation between  $H\alpha$  FWHM and line luminosity is shown below, for the BLAST sample, SMGs (crosses; Swinbank et al. 2004), and normal  $z\sim 2$  galaxies (e.g. LBGs, gray triangles; Erb et al. 2003). The  $H\alpha$  line luminosity is converted to a SFR at right and the  $H\alpha$  FWHM is converted to a virial mass estimate (using the assumption of  $r_{1/2} = 3$  kpc) at top. The BLAST  $250\mu\text{m}$  sample has similarly broad and strong  $H\alpha$  emission to the SMG population, and is brighter than the normal  $z\sim 2$  galaxies. The two galaxies with tentative redshifts are shown as empty circles. This plot suggests that  $250\mu\text{m}$ -luminous galaxies might share intrinsic, physical properties with the SMG population.

$SFR_{\text{FIR}}/SFR_{H\alpha} = 7$ , which is the lowest SFR ratio of the sample indicative of a less  $H\alpha$  obscuration.

We convert the  $[\text{NII}]/H\alpha$  ratios to  $12 + \log(\text{O}/\text{H})$  using the methods described by Maiolino et al. (2008). However two sources (J033249 and J033212) have  $\text{O}/\text{H}$  limits  $> 9.25$ , which corresponds to very strong  $[\text{NII}]/H\alpha$  ( $\gtrsim 0.5$ ). The  $\text{O}/\text{H}$  and  $[\text{NII}]/H\alpha$  indicators saturate at metallicities above solar (see Pettini & Pagel 2004), and additional contribution from either AGN or shocked gas can increase the  $[\text{NII}]/H\alpha$  ratio further (e.g. van Dokkum 2005). The remaining five secure detections have  $12 + \log(\text{O}/\text{H})$  values which average to  $8.64 \pm 0.08$ . The measured  $[\text{NII}]/H\alpha$  ratio for the stacked  $H\alpha$  spectrum implies a metallicity of  $12 + \log(\text{O}/\text{H}) = 8.75^{+0.08}_{-0.10}$  (in agreement with the average for the individual measurements).

## 2.2 Dust SED Fitting and FIR/radio Correlation

We fit the MIPS ( $70\mu\text{m}$ , and  $160\mu\text{m}$ , where available), BLAST ( $250\mu\text{m}$ ,  $350\mu\text{m}$ , and  $500\mu\text{m}$ ), and LABOCA ( $870\mu\text{m}$ ) flux densities to two different FIR dust models. For FIR SED fitting, we correct the BLAST flux densities for boosting by confusion noise as mentioned in the beginning of this section. Both FIR SED models assume a modified blackbody emission curve with a single dust temperature:

$$S_\nu \propto \frac{\nu^{3+\beta}}{\exp(h\nu/kT_{\text{dust}}) - 1} \quad (1)$$

where  $S_\nu$ , the flux density, is a function of rest frequency  $\nu$ , the emissivity  $\beta$ , dust temperature  $T_d$ , and FIR luminosity  $L_{\text{FIR}}$  (which governs the normalisation of the function). The first model allows  $\beta$  to vary (the “beta-free” model) while the second model fixes emissivity to  $\beta = 2$ . Both models

have  $T_d$  and  $L_{\text{FIR}}$  as free parameters. The advantage of allowing emissivity to vary in the first model allows a reassessment of the emissivity constraints which have been placed on ULIRGs in past studies (e.g.  $\beta = 1.5$  or  $2.0$ ; Chapman et al. 2005; Casey et al. 2009c,b; Younger et al. 2009). In addition, our measurements of  $\beta$  are made independent of any *a priori* constraint on  $T_d$  or  $L_{\text{FIR}}$ . We choose to make the second model rigid as fits from the first model can be unphysical, as might be the case if the FIR flux densities are particularly faint or affected by source confusion.

Only J033212 and J033237 are poorly fit to a beta-free model (these are the two galaxies with tentative redshift identifications), since they do not have  $70\mu\text{m}$  data and have unconstraining upper limits in the FIR. We use only the fixed  $\beta = 2$  model for these two. The remaining seven galaxies have reliable beta-free SED fits, and from them we measure  $\beta$ ,  $T_{\text{dust}}$ , and  $L_{\text{FIR}(8-1000\mu\text{m})}$  (summarised in Table 1). Both fixed beta and beta-free fits are shown in Figure 4. We find a mean emissivity of  $\beta = 1.73 \pm 0.13$  and a mean dust temperature of  $T_d = 52 \pm 6$  K.

The FIR luminosities ( $8-1000\mu\text{m}$ ) must be corrected to account for mid-infrared ( $8-25\mu\text{m}$ ) emission from PAH and power law sources (e.g. Menéndez-Delmestre et al. 2009) above the single FIR modified blackbody. We tether the Pope et al. (2008) SMG SED to  $24\mu\text{m}$  flux densities (as seen in Figure 4) to estimate the luminosity deficit of the single temperature blackbody. This deficit varies substantially object to object due to the large spread in  $24\mu\text{m}$  flux densities and blackbody properties in the  $8-25\mu\text{m}$  Wein tail. On average, we find that the contribution of the PAH and AGN emission account for  $0.04 \pm 0.03$  dex of luminosity which we add to the FIR luminosities as a correction factor. Although the mid-IR properties of the sample can vary substantially, this deficit translates to no more than a  $\sim 10\%$  increase in FIR luminosity for these  $> 10^{13} L_\odot$  systems. The corrected luminosities are given in Table 1.

We also overplot the composite SMG spectrum, from Pope et al. (2008), normalised to the integrated  $24\mu\text{m}$  flux density in Figure 4. While the SMG composite is carefully derived based on mid-IR to FIR data of SMGs to date, it fails to fit the BLAST FIR data on a case by case basis. In some cases, it under/overestimates the FIR luminosities by  $\pm 1$  dex. This illustrates how a  $24\mu\text{m}$ -normalised SED fitting procedure, which is common in the literature (e.g. Desai et al. 2009) places poor constraints on the breadth of FIR properties of ULIRG samples, especially in the absence of direct FIR measurements. Recent high-resolution FIR observations (e.g. Younger et al. 2010) have demonstrated that  $24\mu\text{m}$  counterparts are often misidentifications and do not correspond to the FIR luminous source.

Although multiple dust temperature blackbodies are found to fit well to local ULIRGs in the literature (for example, see Clements et al. 2010), strong assumptions must be made regarding the FIR luminosity or normalisation, to decompose the sparse FIR data down into multiple blackbody components. Given the uncertainty of the FIR luminosities or flux densities at any given wavelength, we decide to forgo multiple dust temperature fitting for well constrained, single dust temperature blackbody fits. If multiple blackbodies provide a more physical SED fit, then our derived emissivities, from the single blackbody fits, could be underestimated.

**Table 2.** H $\alpha$  and stellar properties of BLAST 250 $\mu\text{m}$  Galaxies

NAME	$z$	$S_{\text{H}\alpha}$ ( $\text{W m}^{-2}$ )	$L_{\text{H}\alpha}$ ( $10^{35}$ W)	$\text{FWHM}_{\text{H}\alpha}$ ( $\text{km s}^{-1}$ )	$\langle[\text{NII}]/\text{H}\alpha\rangle^a$	$\langle\text{O}/\text{H}\rangle^a$	$\text{SFR}_{\text{H}\alpha}$ ( $\text{M}_{\odot} \text{ yr}^{-1}$ )	$\text{SFR}_{\text{FIR}}$ ( $\text{M}_{\odot} \text{ yr}^{-1}$ )	$\text{SFR}_{\text{radio}}$ ( $\text{M}_{\odot} \text{ yr}^{-1}$ )	$M_{\star}$ ( $\text{M}_{\odot}$ )
J033129	1.482	$4.1 \times 10^{-19}$	$(5.6^{+0.9}_{-0.8})$	$190 \pm 60$	0.13	8.60	$44^{+7}_{-6}$	$2100^{+1100}_{-700}$	$1300^{+440}_{-330}$	$1 \times 10^{10}$
J033151	1.599	...	...	...	...	...	...	$3800^{+2500}_{-1500}$	$1000^{+430}_{-300}$	$3 \times 10^{10}$
J033152	2.342	$1.3 \times 10^{-18}$	$(53^{+3}_{-2})$	$490 \pm 40$	0.74	$> 9.25$	$419^{+20}_{-19}$	$14000^{+10000}_{-6000}$	$28000^{+5200}_{-4400}$	$3 \times 10^{10}$
J033204	2.252	$5.2 \times 10^{-19}$	$(20^{+3}_{-3})$	$360 \pm 40$	0.14	8.64	$154^{+24}_{-21}$	$6800^{+1700}_{-1400}$	$3300^{+1000}_{-800}$	$5 \times 10^{10}$
J033243	2.123	$1.3 \times 10^{-18}$	$(42^{+5}_{-5})$	$800 \pm 50$	0.18	8.71	$335^{+46}_{-40}$	$2400^{+4300}_{-1500}$	$2000^{+720}_{-530}$	$4 \times 10^{10}$
J033246	1.382	$4.2 \times 10^{-19}$	$(4.9^{+0.5}_{-0.5})$	$150 \pm 70$	0.13	8.59	$39^{+4}_{-4}$	$680^{+200}_{-150}$	$650^{+180}_{-140}$	$1 \times 10^{10}$
J033249	2.326	$5.8 \times 10^{-19}$	$(25^{+3}_{-3})$	$360 \pm 50$	0.14	8.64	$194^{+23}_{-20}$	$14000^{+7000}_{-4000}$	$6100^{+1700}_{-1300}$	$3 \times 10^{10}$
J033212	1.93	$3.5 \times 10^{-19}$	$(9.3^{+1.9}_{-1.6})$	$310 \pm 50$	0.55	$> 9.25$	$73^{+15}_{-13}$	$3800^{+7000}_{-2000}$	$< 690$	$4 \times 10^{10}$
J033237	2.64	$1.0 \times 10^{-18}$	$(57^{+9}_{-8})$	$630 \pm 50$	0.33	8.96	$451^{+69}_{-60}$	$6000^{+13000}_{-4000}$	$6700^{+1500}_{-1200}$	$9 \times 10^{10}$

**Table Notes.** H $\alpha$  properties from VLT-ISAAC spectra of the BLAST 250 $\mu\text{m}$  sample. The seven at top have secure redshifts (the six which have H $\alpha$  properties are used in our analysis) while the bottom two have tentative redshifts (we calculate their H $\alpha$  properties, but exclude them from aggregate property analysis in section 3 despite being illustrated in figures). FWHM has been deconvolved with the instrumental resolution measured from skylines in the vicinity of H $\alpha$  ( $\sim 6.5\text{\AA}$  in K-band and  $\sim 4.4\text{\AA}$  in H-band), and SFR is derived from  $L_{\text{H}\alpha}$  using the relation  $\text{SFR} = 7.9 \times 10^{-35} L_{\text{H}\alpha}$  from Kennicutt (1998). The metallicity measurements (<sup>a</sup>) are computed by  $\langle[\text{NII}/\text{H}\alpha]\rangle = \log(S_{\text{NII}}/S_{\text{H}\alpha})$  and  $\langle\text{O}/\text{H}\rangle = 12 + \log(\text{O}/\text{H})$  derived from  $\langle[\text{NII}/\text{H}\alpha]\rangle$  using methods described in Maiolino et al. (2008). The characteristic uncertainty on  $[\text{NII}]/\text{H}\alpha$  is  $\sim 0.10$ . Stellar masses (<sup>b</sup>) are measured from *Spitzer*-IRAC photometry which brackets the rest-1.6 $\mu\text{m}$  stellar bump (see § 2); the characteristic uncertainty in stellar mass is  $\sim 2 \times 10^{10} \text{M}_{\odot}$ .

We measure  $q_{\text{IR}}$ , the ratio of integrated IR flux to radio flux, as described in detail by I10 to verify the FIR/radio correlation in our sample. I10 finds a mean  $q_{\text{IR}} = 2.41 \pm 0.20$  based on the larger sample of BLAST sources with photometric redshifts. Assuming a radio synchrotron slope of  $\alpha = 0.75$ , we measure a mean  $q_{\text{IR}} = 2.46 \pm 0.18$  which agrees with I10 and earlier findings (e.g. Dale et al. 2007) that there is no evidence for evolution in  $q_{\text{IR}}$  with redshift. Since  $\alpha$  has a significant impact on the calculation of  $q_{\text{IR}}$ , we consider the impact of variations in  $\alpha$ : I10 explicitly measured  $\alpha$  for a high-redshift subset of their BLAST sample and found a median value of  $\alpha = 0.4$ . If we use  $\alpha = 0.4$  instead to calculate  $q_{\text{IR}}$  we measure  $q_{\text{IR}} = 2.27 \pm 0.17$ . This is still in agreement with I10's measurement of the FIR-radio correlation at high redshift within uncertainties.

We note that Kovács et al. (2006) concluded that the local FIR/radio correlation *overestimates* FIR luminosity by factors of  $\sim 0.2$ - $0.4$  dex for SMGs, which contrasts with our and I10's result for BLAST sources. However, the difference is due to different FIR SED fitting procedures; when we refit the 21 SMG FIR points (measured at 350 $\mu\text{m}$  and 850 $\mu\text{m}$ ) in Kovács et al. (2006) using the methods described in this paper (for fixed  $\beta = 1.5$ ) we find  $q_{\text{IR}} = 2.46 \pm 0.19$ . Figure 5 shows the flux densities of the BLAST sample in the FIR-radio context, plotted against two template SEDs which follow the relation: an M82 template (Bressan et al. 2002) and a composite SMG SED (Pope et al. 2008). Some sources exceed the relation (often due to flux excesses towards shorter wavelengths) while others' FIR luminosities are over-predicted, most likely due to AGN contribution to radio luminosity (e.g. J033152). However, these variations do not appear to be weighted in either direction, indicating that the FIR/radio correlation is predicting FIR luminosities accurately for the population on a whole.

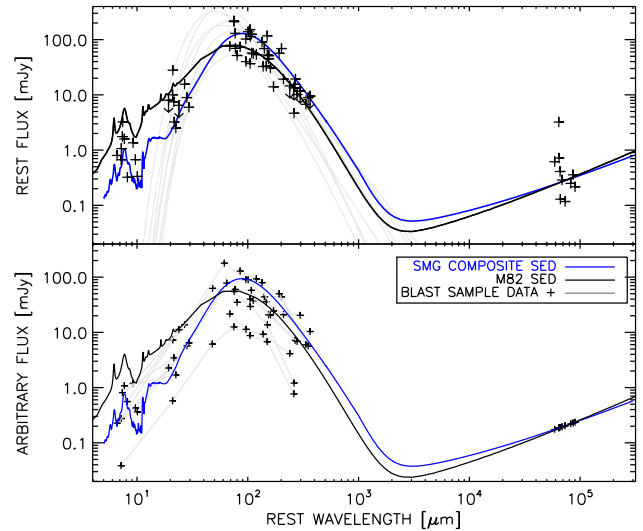


**Figure 5.** A comparison of the BLAST FIR and radio flux densities against two template SEDs: an M82 spectrum (black) from (Bressan et al. 2002) and a composite SMG spectrum (blue) taken from Pope et al. (2008). The upper panel plots all sources' flux densities in their rest-frame (with overplotted best-fit FIR SEDs (light gray) from Fig. 4). The lower panel plots all sources with fluxes renormalised to their radio points. The scatter around the template SEDs in the lower panel (where the flux has been renormalised to the radio) indicates our observed variation in the FIR-radio correlation. While there appears to be a large scatter, there is no systematic offset from the FIR-radio predicted FIR luminosities and those measured directly in our sample.

### 3 DISCUSSION

Combining the unique BLAST FIR data with previous *Spitzer* observations and our spectroscopic redshift iden-

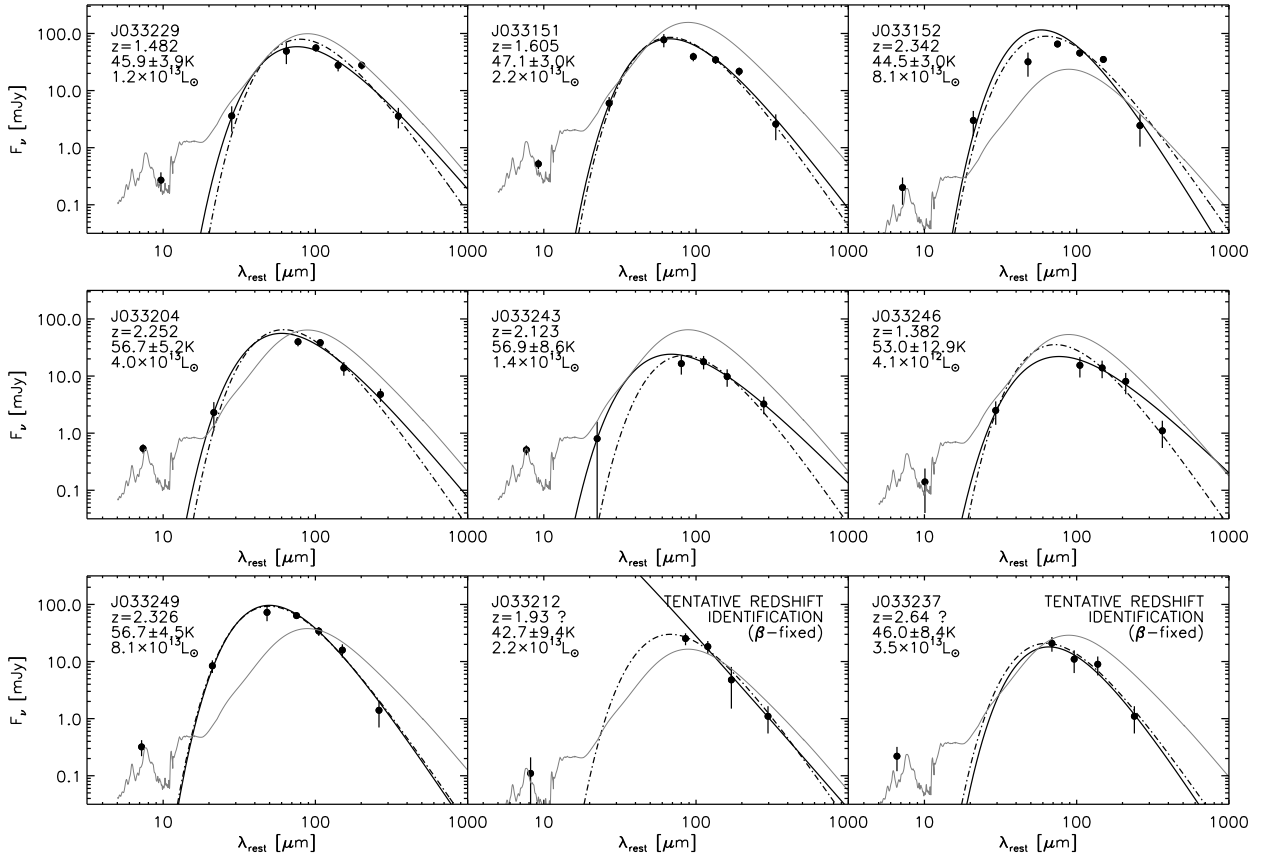


**Figure 4.** The FIR SEDs for high- $z$  BLAST sources, including data from *Spitzer*-MIPS ( $24\mu\text{m}$ , and  $70\mu\text{m}$ ,  $160\mu\text{m}$  where available), BLAST ( $250\mu\text{m}$ ,  $350\mu\text{m}$ , and  $500\mu\text{m}$ ) and LABOCA ( $870\mu\text{m}$ ). We fit three SEDs to the data: (1) a single dust temperature with fixed  $\beta = 2$  modified blackbody as in Eq. 1 (dashed-dotted line), (2) a modified blackbody with  $\beta$  treated as a free parameter (solid black line), and (3) an SMG composite SED from Pope et al. (2008) normalised to  $24\mu\text{m}$  flux density (thin gray line). The galaxies’ names, redshifts, best fit dust temperatures, and FIR luminosities are inset on each SED plot. The two galaxies marked TENTATIVE (from their tentative redshift identifications) are also the two galaxies whose fixed  $\beta = 2$  SED fit was significantly better than the beta-free model. Neither tentative galaxies are included in the analysis of section 3

tifications allows a full characterisation of FIR SEDs for  $250\mu\text{m}$ -bright HyLIRGs. Since  $250\mu\text{m}$  mapping has the advantage of sampling blackbody emission near its peak at  $z \sim 2$ ,  $250\mu\text{m}$  ULIRG/HyLIRG selection is far less biased towards certain SED shapes, making  $250\mu\text{m}$ -bright galaxies a much cleaner, unbiased subset all high-redshift ULIRGs.

### 3.1 Source Density

The seven galaxies with secure redshifts suggest that these  $250\mu\text{m}$ -bright galaxies have roughly  $1/5$  the volume density of similarly luminous SMGs. We exclude the sources which only have tentative redshift identifications from this analysis, although we note that they would not skew or affect the interpretations we draw from the entire sample. We estimate this lower limit to  $\rho_{250}$  for our sample by taking the redshift ranges  $z = 1.3 - 1.7$  and  $z = 2.0 - 2.6$ , given the gap in the atmospheric opacity between  $H$  and  $K$ -bands. We treat the D10 and I10 sample separately as the relative selection depths differ ( $S_{250} > 33 \text{ mJy}$  and  $S_{250} > 59 \text{ mJy}$

respectively), finding  $> 8 \times 10^{-6} \text{ h}^3 \text{ Mpc}^{-3}$  and  $> 5 \times 10^{-6} \text{ h}^3 \text{ Mpc}^{-3}$  respectively. Of the spectroscopically identified SMG samples in the literature (e.g. Chapman et al. 2005), 51% of the sources have  $L_{\text{FIR}} > 8 \times 10^{12} L_{\odot}$  (a cutoff corresponding approximately to the BLAST  $250\mu\text{m}$  depth), which implies a luminosity-limited volume density of  $2.5 \times 10^{-5} \text{ h}^3 \text{ Mpc}^{-3}$  for SMGs. As much deeper, more uniform  $250\mu\text{m}$  data become available from *Herschel*, the overlap with the SMG population is being explored more fully (e.g. Elbaz et al. 2010).

Of our nine spectroscopic sources, only four have been detected as SMGs in Weiß et al. (2009). While  $250\mu\text{m}$ -bright sources at high- $z$  are more rare than SMGs, the fact that 55% (5/9) of our sample are submm-faint (with  $\langle S_{870} \rangle \lesssim 2 \text{ mJy}$ ) highlights that the SMG population represents only a subset of high-redshift ULIRG activity, as Casey et al. (2009), Chapman et al. (2004) and Blain et al. (2004) suggest. The addition of  $250\mu\text{m}$ -selected, submm-faint galaxies to the previously-known HyLIRG population could imply that the volume density of known high- $z$

HyLIRGs would increase from the SMG estimate roughly by  $\gtrsim 12\%$ . However, more spectral observations of similar 250 $\mu\text{m}$ -bright objects from *Herschel* are needed to boost these statistics and understand the actual level of contribution.

### 3.2 Near-infrared Spectral Features

The H $\alpha$  derived star formation rates of the BLAST HyLIRG sample underestimate the FIR SFRs by  $\sim 10\times$ , as is often the case with rest-UV or rest-optical emission line star-formation indicators in dust-obscured starburst galaxies. However, we note near-IR spectroscopic observations of SMGs in Takata et al. (2006) measured internal extinction factors of  $A_V = 2.9 \pm 0.5$  using H $\alpha$ /H $\beta$  ratios. When correcting the H $\alpha$ -inferred SFRs in Table 2 for this dust extinction the FIR-inferred SFRs are recovered, averaging to  $\sim 2000 M_\odot \text{ yr}^{-1}$ . This indicates that dust obscuration is significant in the near-IR and must be corrected for to understand the true nature of the ultraluminous activity in these galaxies.

Placing our [NII]/H $\alpha$  metallicity measurements in a larger galaxy evolution context, the metallicities of this sample (measured by converting to  $\langle \text{O}/\text{H} \rangle$ , i.e.  $\langle 12 + \log(\text{O}/\text{H}) \rangle = 8.65$ ), agree within uncertainties with the observed metallicities of the most massive  $z \sim 2$  galaxies,  $\langle 12 + \log(\text{O}/\text{H}) \rangle \sim 8.55 \pm 0.07$ , in Erb et al. (2006). The mean [NII]/H $\alpha$  ratio for this sample,  $0.29 \pm 0.23$ , agrees within uncertainty with the Swinbank et al. (2004) SMGs,  $0.41 \pm 0.38$ . While evolutionary conclusions should not be drawn from these data alone, the results are consistent with conjecture that the ULIRG phenomenon occurs at the early stages of a burst in star formation triggered by the merger of two typical gas-rich massive galaxies at  $z \sim 2$ .

### 3.3 Temperature Fitting and Selection

Figure 6 shows dust temperature ( $T_{\text{dust}}$ ) against FIR luminosity, with BLAST 250 $\mu\text{m}$  sources and SMGs overplotted. Representative  $1\sigma$  detection boundaries at 70 $\mu\text{m}$ , 250 $\mu\text{m}$  and 870 $\mu\text{m}$  are shown to illustrate the populations' selection biases ( $2\sigma$ ,  $3\sigma$  or  $5\sigma$  detection limits would have the same shape but be shifted to the right in luminosity; e.g. the  $3\sigma$  detection limit corresponds to a luminosity shift of  $\sim 0.4$  dex). The mean dust temperature of our sample, when fit with single modified blackbody SEDs, is  $52 \pm 6$  K, which is comparable to the mean dust temperature of local ULIRGs of similar ( $\gtrsim 10^{13} L_\odot$ ) luminosities,  $45 \pm 10$  K (Chapman et al. 2003; Rieke et al. 2009), and only  $\sim 5$  K warmer than SMGs of similar luminosities  $> 10^{13} L_\odot$  (and is 15 K warmer than SMGs on average, which are  $36 \pm 7$  K). Overall, all BLAST sources (except the lower-redshift J033246) have dust temperatures consistent with the high luminosity end of the SMG distribution.

It is important to note that the SMG FIR luminosities shown here are derived from radio luminosity, via the FIR/radio correlation, and that the associated dust temperature fits are reliant upon that assumption. To first order, we and others have shown that the FIR/radio correlation holds at these redshifts and luminosities (for direct comparison see Table 2), however scatter is significant, with differences in measured/derived FIR luminosities of  $\pm 0.7$  dex. As

is often done for literature SMGs to date (Chapman et al. 2005), dust temperature is measured by using a single FIR data point (e.g. observed 850 $\mu\text{m}$ ) and forcing an SED with fixed radio-inferred  $L_{\text{FIR}}$ . If the radio-inferred FIR luminosity is significantly different from the actual FIR luminosity, then the dust temperature will either be grossly over- or underestimated.

We use the BLAST sample and its full SED information (thus directly measuring FIR luminosity) to test the accuracy of FIR fits and derived dust temperature for SMGs and other high- $z$  ULIRGs. Regardless of the accuracy of radio-derived FIR luminosities, we find that  $T_{\text{dust}}$  is systematically underestimated by  $12 \pm 19$  K when derived from 870 $\mu\text{m}$  flux densities. Similarly, we also measure dust temperature from the 70 $\mu\text{m}$  flux densities (as is done in Casey et al. 2009c, for 70 $\mu\text{m}$ -luminous radio galaxies), and find that they are overestimated systematically by  $6 \pm 10$  K.

The severity of these over- and under predicted dust temperatures is due in part to the sample selection. Because the sample is selected at 250 $\mu\text{m}$ , it is likely that considering only the 870 $\mu\text{m}$  or 70 $\mu\text{m}$  points will produce larger  $T_d$  error than the 870 $\mu\text{m}$  or 70 $\mu\text{m}$  selected samples, simply because of the temperature-weighting and biasing of these selection wavelengths. In other words, if a galaxy is 870 $\mu\text{m}$ -bright and is 250 $\mu\text{m}$ -faint, then it is far more likely to have a cooler inherent temperature than a galaxy which is bright at both wavelengths. This highlights the difficulty with fitting dust temperatures to single FIR flux measurements and demonstrates that the luminosity-temperature distribution of previously studied ULIRG populations should be revisited when more complete SED information is gathered from *Herschel* and SCUBA-2 (e.g. Magnelli et al. 2010).

### 3.4 HyLIRG Evolution

Figure 6 highlights where 250 $\mu\text{m}$  observations are more sensitive to hotter dust temperatures than  $\sim 870\mu\text{m}$  at  $z > 1$ . The sparsity of detections in the highlighted region of Fig. 6 indicates that hot-dust HyLIRGs are genuinely much more rare than their cold-dust analogues at  $L_{\text{FIR}} > 10^{13} L_\odot$  at high redshift.

The dearth of hot-dust ULIRGs ( $\gtrsim 60$  K) from these data is only significant in the HyLIRG ( $> 10^{13} L_\odot$ ) regime for redshifts above  $z = 1.5$  (in other words, it is also significant at fainter luminosities at lower redshifts but not fainter luminosities at high redshifts). Due to the 250 $\mu\text{m}$  BLAST sensitivity, we have only one  $10^{12} < L_{\text{FIR}} < 10^{13} L_\odot$  ULIRG in our sample, and its redshift is  $\sim 1.3$ . This leaves the possibility that  $z \sim 2$  hotter-dust ULIRGs exist, but lie beneath current 250 $\mu\text{m}$  imaging depth. Casey et al. (2009c) showed that at slightly lower redshifts,  $z \sim 1.5$ , star-formation dominated hot-dust ULIRGs ( $T_d \sim 52$  K,  $L_{\text{FIR}} \gtrsim 2 \times 10^{12} L_\odot$ ) have been observed at 1/5 the volume density of SMGs, but limitations in *Spitzer*-MIPS 70 $\mu\text{m}$  depth prevented significant detections at  $z \gtrsim 2$ . Also, work by Casey et al. (2009a) argues that hotter-dust  $> 60$  K HyLIRGs at  $z \sim 2$  are less prevalent based on CO observations of submm-faint radio galaxies. After accounting for selection bias, the submm-faint ULIRG sample was  $\sim 2\times$  less luminous in  $L_{\text{FIR}}$  and  $L_{\text{CO}}$  than CO-observed, cold-dust SMGs.

If we assume *a priori* that high- $z$  ULIRGs have the same dust temperature distribution as local ULIRGs (which

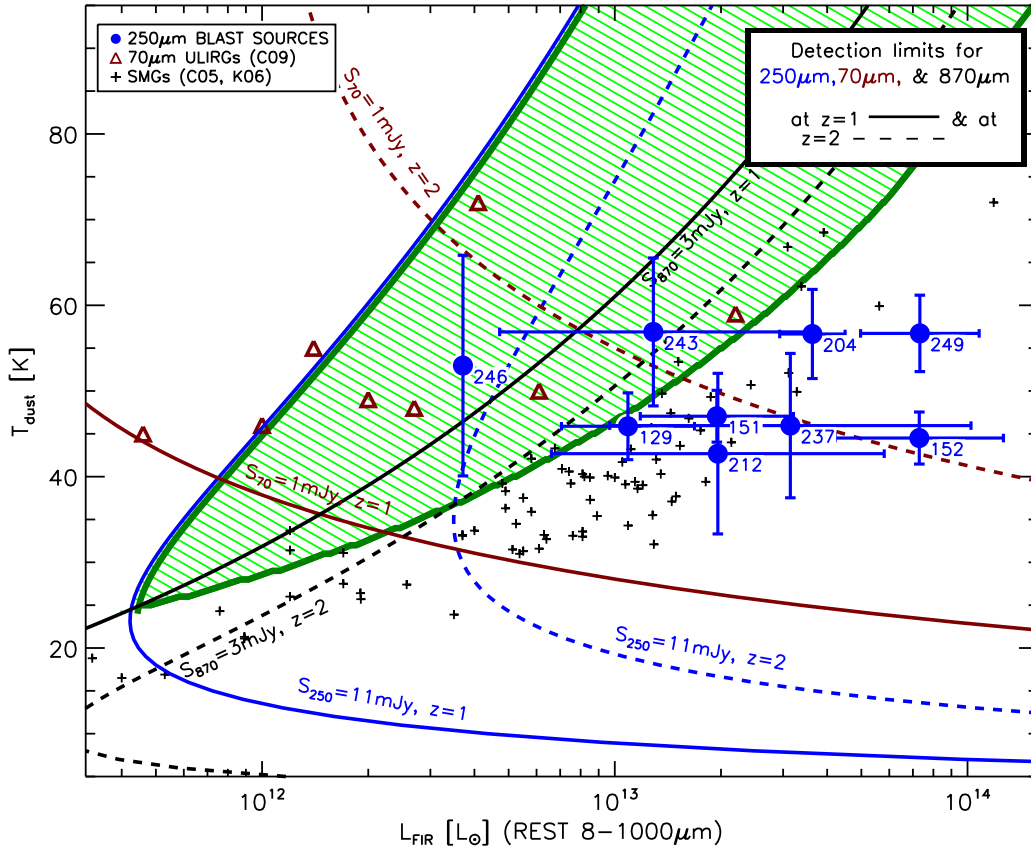


**Figure 6.** FIR luminosity against dust temperature for the BLAST 250 $\mu\text{m}$  sample (blue circles, labelled by the last three digits in their right ascension). The dashed ( $z = 2$ ) and dotted ( $z = 1$ ) lines indicate rough 1- $\sigma$  boundaries at 250 $\mu\text{m}$  (blue,  $\sigma_{250}=11\text{mJy}$ , BLAST), 70 $\mu\text{m}$  (red,  $\sigma_{70}=1\text{mJy}$ , MIPS), and 870 $\mu\text{m}$  (black,  $\sigma_{870}=3\text{mJy}$ , LABOCA), where sources at the given redshift would have 1- $\sigma$  significance if it has  $L_{\text{FIR}}$  and  $T_{\text{d}}$  corresponding to the boundary, and would be  $>1\sigma$  if it lies to the right of the boundary. To translate these curves into 3- $\sigma$  detection limits, they would be shifted  $\sim 0.4$  dex to the right in luminosity space; the shape of the boundary curves would be maintained. 70 $\mu\text{m}$ -bright “hot-dust” ULIRGs from Casey et al. (2009c) are overlaid as red triangles. The 850 $\mu\text{m}$ -detected SMGs from Chapman et al. (2005) and Kovács et al. (2006) are overlaid as small black crosses. The area enclosed by the green highlights a phase-space where 250 $\mu\text{m}$  observations are more sensitive than 870 $\mu\text{m}$  at all redshifts  $z > 1$ .

have  $\langle T_{\text{d}} \rangle = 45 \pm 10$  K above  $10^{13}$  K), then there is a  $\sim 60\%$  chance that no  $>60$  K sources are detected within a sample of seven sources (given a Gaussian distribution of dust temperatures for systems  $>10^{13}$   $L_{\odot}$ ). This illustrates how limiting our sample size is when it comes to drawing conclusions for the whole 250 $\mu\text{m}$ -luminous population. For example, a sample of  $\sim 30$  sources with  $T_{\text{dust}} < 60$  K must be detected in order for that likelihood to drop to  $\lesssim 13\%$ . More spectroscopic observations and FIR characterisations of similar samples are needed from *Herschel* and SCUBA-2 for real progress to be made in high- $z$  ULIRG evolutionary studies, and to probe the differences with local ULIRG populations.

Despite its significant uncertainty given the small sample size, the lack of hot-dust systems ( $>60$  K) in the BLAST HyLIRG sample is consistent with predictions from SPH simulations for infrared luminous galaxies (see Narayanan et al. 2009). They suggest that the brightest high- $z$  starbursts ( $>10^{13}$   $L_{\odot}$ ) are at their most active phase during the early stages of final merger in-fall, when gas and dust are diffuse, extended, and cold. Warmer dust is sug-

gested to condense either at a later stage merger, when gas and dust has collapsed and heated, or when it has been heated by a growing AGN. While this sample of galaxies exhibits warm dust ( $30 < T_{\text{dust}} < 50$  K), we have not detected any  $>10^{13}$   $L_{\odot}$  hot-dust ( $>60$  K) systems in this sample and we find a modest AGN fraction (20%); therefore, our results loosely support the theory that the most luminous HyLIRGs are triggered by major merging events.

### 3.5 Confusion

It is important to once again consider the impact of confusion limitations and deboosting factors on our conclusions. We excluded the uncertainty in the deboosting factor from our results (as discussed in § 2) because its blind propagation into all of the bands in our SED fits is not justified. As is discussed, the deboosting uncertainty is likely to have far greater effect on  $L_{\text{FIR}}$  than on  $T_{\text{d}}$  or  $\beta$  since boosting is correlated between FIR bands. Using a naive model where the main contribution to source confusion is a single addi-

tional source within the beam, whose FIR colours have the same distribution as seen in *Herschel* populations, we estimate that the derived  $L_{\text{FIR}}$  is uncertain by  $\sim 0.1$  dex and  $T_{\text{dust}}$  is uncertain by  $\sim 9$  K. However, without a proper understanding of the sources which boost the flux of our high- $z$  BLAST sample, it is very difficult to determine how the dust temperatures might change, although it is unlikely that the mean would shift far from the current mean,  $52 \pm 6$  K. This differential boosting issue should be investigated carefully with future, large *Herschel* 250 $\mu$ m-selected samples.

The deboosting effect on luminosity is easier to quantify than the effect on  $T_d$ . The maximum uncertainty for the deboosting factor found by Eales et al. (2009) is  $\sim 50\%$ , which would propagate to a factor of  $\sim 2$  in luminosity. The mean luminosity of our sample is  $\sim 3 \times 10^{13} L_{\odot}$ , a factor of  $\sim 5$ -10 greater than most high- $z$  ULIRG populations in the literature. The factor  $\sim 2$  difference caused by potential deboosting corrections is not significant in comparison. These 250 $\mu$ m-bright galaxies are still ‘‘HyLIRGs,’’ thus amongst the most luminous, extreme starbursts measured at high-redshift.

#### 4 CONCLUSIONS

The redshift identification of these 250 $\mu$ m-bright,  $z \sim 2$  HyLIRGs has allowed a characterisation of their near-IR and FIR properties, leading to the following conclusions:

Near-IR spectroscopy (as probed here by VLT ISAAC) is an efficient way of identifying redshifts (50-70% success rates) for FIR sources which have secure photometric redshifts. The redshift range of our sample is  $z = 1.3$ -2.6, averaging to  $\langle z \rangle = 2.0 \pm 0.4$ , making up the  $z \gtrsim 1$  subset of 250 $\mu$ m-bright BLAST galaxies. We also find that H $\alpha$  star formation rates underpredict their FIR SFRs by  $\sim 35$  times, and we measure metallicities which are in agreement with other high- $z$  galaxy samples, include those of much lower luminosities but of similar stellar mass.

Having multiple FIR flux densities available for each object, we fit FIR blackbody SEDs to each source and constrain  $L_{\text{FIR}}$ ,  $T_d$ , and  $\beta$  independent of radio flux density or mid-IR flux densities. We find that the FIR/radio correlation holds, but that SMG composite spectra, when fit to 24 $\mu$ m flux densities, do not successfully describe the FIR properties of this sample. We measure FIR luminosities  $\sim 3 \times 10^{13} L_{\odot}$ , and dust temperatures averaging  $T_{\text{dust}} = 52 \pm 6$  K. However, we warn that both of these conclusions are sensitive to the effects of flux boosting in the FIR, although we estimate that this should not change  $L_{\text{FIR}}$  by more than a factor of  $\sim 2 \times$  and  $T_{\text{dust}}$  beyond its quoted error.

Since 250 $\mu$ m selection is more sensitive to the detection of hotter dust sources than SMG selection (at 850 $\mu$ m), the lack of  $> 60$  K hot-dust galaxies in our sample is potentially an indication that high- $z$ , high- $L$  galaxies are more extended (with diffuse, cool dust) on a whole than local ULIRGs. However our small sample size limits this conclusion to only  $\lesssim 40\%$  likelihood. A lack of  $> 60$  K hot-dust specimens in the BLAST 250 $\mu$ m population could be telling to the galaxies’ evolutionary stage; this work highlights the need for more observations of larger samples of similar and fainter sources. FIR mapping at 70-500 $\mu$ m from *Herschel* and SCUBA2 will further select rare and poorly studied high-

$z$  ULIRG populations like the galaxies presented here, and near-IR spectroscopic observations will enable further redshift identification of their counterparts, leading to a better characterisation of the ULIRG phenomenon at high- $z$ .

#### ACKNOWLEDGMENTS

We thank Rob Ivison and Jim Dunlop for their help in the analysis and their comments on this manuscript. We also thank the anonymous referee for many helpful suggestions which improved the paper. Based on observations made with ESO Telescopes under programme numbers 082.A-0890, 083.A-0666, and 084.A-0192. CMC thanks the Gates Cambridge Trust, and IRS thanks STFC for support.

#### REFERENCES

- Amblard A., et al., 2010, ArXiv e-prints  
 Blain A. W., Chapman S. C., Smail I., Ivison R., 2004, ApJ, 611, 725  
 Bressan A., Silva L., Granato G. L., 2002, A&A, 392, 377  
 Bussmann R. S., et al., 2009, ApJ, 705, 184  
 Casey C. M., Chapman S. C., Muxlow T. W. B., Beswick R. J., Alexander D. M., Conselice C. J., 2009, MNRAS, 395, 1249  
 Casey C. M., et al., 2009a, MNRAS, p. submitted  
 Casey C. M., et al., 2009b, MNRAS, 400, 670  
 Casey C. M., et al., 2009c, MNRAS, 399, 121  
 Chapin E., et al., 2010, ArXiv e-prints  
 Chapman S. C., Blain A. W., Smail I., Ivison R. J., 2005, ApJ, 622, 772  
 Chapman S. C., Helou G., Lewis G. F., Dale D. A., 2003, ApJ, 588, 186  
 Chapman S. C., Smail I., Blain A. W., Ivison R. J., 2004, ApJ, 614, 671  
 Clements D. L., Dunne L., Eales S. A., 2010, MNRAS, 403, 274  
 Dale D. A., et al., 2007, ApJ, 655, 863  
 Desai V., et al., 2009, ApJ, 700, 1190  
 Devlin M. J., et al., 2009, Nature, 458, 737  
 Dey A., et al., 2008, ApJ, 677, 943  
 Dunlop J. S., et al., 2009, ArXiv e-prints  
 Eales S., et al., 2009, ApJ, 707, 1779  
 Eales S., Lilly S., Webb T., Dunne L., Gear W., Clements D., Yun M., 2000, AJ, 120, 2244  
 Elbaz D., et al., 2010, A&A, 518, L29+  
 Erb D. K., Shapley A. E., Steidel C. C., Pettini M., Adelberger K. L., Hunt M. P., Moorwood A. F. M., Cuby J., 2003, ApJ, 591, 101  
 Erb D. K., Steidel C. C., Shapley A. E., Pettini M., Reddy N. A., Adelberger K. L., 2006, ApJ, 647, 128  
 Gawiser E., et al., 2006, ApJL, 642, L13  
 Hainline L. J., Blain A. W., Smail I., Frayer D. T., Chapman S. C., Ivison R. J., Alexander D. M., 2009, ApJ, 699, 1610  
 Helou G., Soifer B. T., Rowan-Robinson M., 1985, ApJL, 298, L7  
 Hinshaw G., et al., 2009, ApJS, 180, 225  
 Ivison R. J., et al., 2010, MNRAS, 402, 245  
 Kennicutt Jr. R. C., 1998, ApJ, 498, 541

- Kovács A., Chapman S. C., Dowell C. D., Blain A. W., Ivison R. J., Smail I., Phillips T. G., 2006, *ApJ*, 650, 592
- Kriek M., et al., 2008, *ApJ*, 677, 219
- Magnelli B., et al., 2010, *A&A*, 518, L28+
- Maiolino R., et al., 2008, *A&A*, 488, 463
- Menéndez-Delmestre K., et al., 2009, *ApJ*, 699, 667
- Narayanan D., Cox T. J., Hayward C., Younger J. D., Hernquist L., 2009, *MNRAS*, 400, 1919
- Pascale E., et al., 2008, *ApJ*, 681, 400
- Pettini M., Pagel B. E. J., 2004, *MNRAS*, 348, L59
- Pope A., Chary R.-R., Alexander D. M., Armus L., Dickinson M., Elbaz D., Frayer D., Scott D., Teplitz H., 2008, *ApJ*, 675, 1171
- Rieke G. H., Alonso-Herrero A., Weiner B. J., Perez-Gonzalez P. G., Blaylock M., Donley J. L., Marcillac D., . 2009, *ApJ*, 692, 556
- Swinbank A. M., Smail I., Chapman S. C., Blain A. W., Ivison R. J., Keel W. C., 2004, *ApJ*, 617, 64
- Takata T., Sekiguchi K., Smail I., Chapman S. C., Geach J. E., Swinbank A. M., Blain A., Ivison R. J., 2006, *ApJ*, 651, 713
- van Dokkum P. G., 2005, *AJ*, 130, 2647
- Vanzella E., et al., 2008, *A&A*, 478, 83
- Weiß A., et al., 2009, *ApJ*, 707, 1201
- Younger J. D., et al., 2009, *MNRAS*, 394, 1685
- Younger J. D., et al., 2010, *MNRAS*, 407, 1268